

Growth signatures of rosette plants from time-lapse video

Babette Dellen¹, Hanno Scharr², and Carme Torras³, *Senior Member, IEEE*

Abstract—Plant growth is a dynamic process, and the precise course of events during early plant development is of major interest for plant research. In this work, we investigate the growth of rosette plants by processing time-lapse videos of growing plants, where we use *Nicotiana tabacum* (tobacco) as a model plant. In each frame of the video sequences, potential leaves are detected using a leaf-shape model. These detections are prone to errors due to the complex shape of plants and their changing appearance in the image, depending on leaf movement, leaf growth, and illumination conditions. To cope with this problem, we employ a novel graph-based tracking algorithm which can bridge gaps in the sequence by linking leaf detections across a range of neighboring frames. We use the overlap of fitted leaf models as a pairwise similarity measure, and forbid graph edges that would link leaf detections within a single frame. We tested the method on a set of tobacco-plant growth sequences, and could track the first leaves of the plant, including partially or temporarily occluded ones, along complete sequences, demonstrating the applicability of the method to automatic plant growth analysis. All seedlings displayed approximately the same growth behavior, and a characteristic growth signature was found.

I. INTRODUCTION

According to [1] ‘*a key goal of biology is to understand phenotypic characteristics, such as health, disease and evolutionary fitness. Phenotypic variation is produced through a complex web of interactions between genotype and environment, and such a ‘genotype -phenotype’ map is inaccessible without the detailed phenotypic data that allow these interactions to be studied.*’ Plant seedlings display a rich dynamic behavior when watching their growth in time-lapse videos. Two types of changes are commonly observed, leaf growth and nastic leaf movements (see Fig. 1(a) and (b), respectively). Tobacco leaves grow at different rates and can double or even quadruple their size within a day. Nastic leaf movements, characterized by a leaf changing its angular orientation in a periodic manner, occur on a faster time scale, following a day-night rhythm. In the so called *functional approach* to plant growth analysis [2], [3], [4] plant growth and nastic-leaf-movements patterns are derived by fitting model functions to observed shape and pose changes. The model parameters provide specific information about the plants growth behavior and can be used to better understand interdependencies between plant growth, environmental conditions and other preconditions, such as the genotype of the plant [5], [6], [7]. In typical experiments where

individual leaves are investigated, rather than whole shoots, leaf sizes are usually measured manually at regular time intervals [8], [7], [9], using rotating displacement transducers attached to each leaf by a string [10], [11], or cameras looking at leaves stretched out by strings [12], [13], [11]. Taking such measurements over a period of several weeks for a set of plants thus takes considerable effort. Machine vision would be highly useful for this purpose since in current plant phenotyping experiments or in plant production such measurements would have to be conducted for a large number of plants [14], [15], particularly for high-throughput phenotyping. One major problem here arises from the complex appearance of plants, which makes it hard to extract relevant plant features.

More specifically, we are interested in detecting and recognizing the leaves of tobacco seedlings in infrared videos, acquired with a camera monitoring the plant from the top, modeling their shape, and following the individual leaves over time in order to analyze their growth pattern. Unfortunately, true leaf boundaries are hard to detect due to leaves occluding each other and the varying appearance of the leaf in the image, caused by changes in illumination conditions (as they do occur in real settings) or the orientation of the leaf with respect to the camera (due to nastic leaf movements). As a consequence, most procedures for leaf recognition and classification are at least to some degree prone to failure, or require the concurrence of a user to correctly segment and characterize individual leaves [16], [17], [18], [19], [20], [21], [22], [23]. For recognizing and segmenting larger leaves, depth images may help [24]. Previous approaches used only unambiguously identified leaves for tracking to analyze growth, thus avoiding the tracking problem [25], [26], or tracked the entire rosette of a plant [27]. The problem of tracking multiple leaves given ambiguous and noisy measurements was not addressed by these works. Measuring and modeling the growth of all leaves at once, instead of selecting individual leaves beforehand, provides additional information about a plant, e.g. its phyllochrons, i.e. the durations between leaf emergences. They are typically measured as differences between time points when leaves reach a certain size, e.g., length 1cm in [28, cmp. Figure 5].

Towards this goal, we developed a graph-based method for detection and tracking of tobacco leaves from infrared image sequences. First, edges are detected in each image and used to extract smooth contour segments. Next, contour segments are grouped using a leaf-shape model. From the shape model, pairwise similarities of contour segments are computed across frames and used to create a graph. By incorporating a unique-matching constraint into a method for finding the minimum

¹ University of Applied Sciences, RheinAhrCampus, Department of Mathematics and Technology, 53424 Remagen, Germany, dellen@hs-koblenz.de

² IBG-2: Plant Sciences, Forschungszentrum Jülich, 52425 Jülich, Germany

³ Institut de Robòtica i Informàtica Industrial (CSIC-UPC), Llorens i Artigas 4-6, 08028 Barcelona, Spain, torras@iri.upc.edu

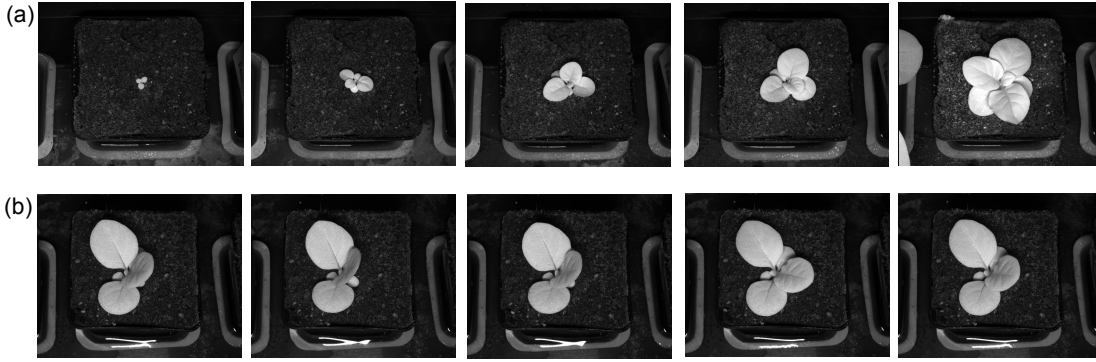


Fig. 1. (a) Infrared images showing the growth of a tobacco seedling over a time interval of 12.5 days. (b) Infrared images showing typical nyctinastic leaf movements taking place over a time interval of only a few hours. These leaf movements are very fast compared to the changes of the leaf induced by growth.

spanning tree in a graph, the main leaf tracks are identified [29]. Gaps in the sequences, i.e., missing leaves, either caused by the motion of the leaves and occlusions, and incorrect leaf detections, leading to false positives, are accommodated by having graph edges that span across several frames. The tracked leaves together with the fitted leaf models provide then information about the growth of individual leaves.

II. METHODS

A. Image acquisition

For image acquisition a black-and-white 5 MP camera with infrared filter blocking out visible light has been used. Images of a resolution of 2448×2048 pixels have been taken at regular, hourly time intervals for each plant over a time period of 12.5 days, and downsized by a factor 2 for faster processing. The tobacco plants showed growth rates of about 35% a day under artificial illumination. All ten tobacco plants used in the experiments were of the same genotype and grown under similar environmental conditions.

To scan a 2D grid with a camera we needed 2 linear moving stages. To perform automatic watering, another moving stage and a lab-pump was needed. Overall, including camera, computer, optical lenses etc. setting up a system should be doable in the range of €10-12k.

B. Edge detection and extraction of contour segments

The goal of this step is to extract elementary contour segments from the images that represent straight or smoothly curved lines for leaf detection. First, we compute an edge map of the image $I(x, y)$ by applying a Canny edge detector (see Fig. 2(a)). In the edge image, we identify junction points, i.e., points that have more than two direct neighbors in the edge images, and disconnect the junction by setting the edge map to zero at the junction point. We assign a unique label to each connected group of edge points. For this, we start at one of the corner points (having only one direct neighbor) of an edge and walk along the edge until the second corner point is reached. If no corner point is found (closed contour), we start at an arbitrary point and stop when we are back to the starting point. Each of these connected groups defines a contour segment, containing an ordered list of points (x, y) from the start point

to the end point of the contour. We then break the contour segments further down into smooth, primitive line segments with the aim of disconnecting contour segments belonging to different leaves. This way, an adequate leaf-shape model can be fitted to the primitives in the next step (see Section II-C). For this, we fit a polynomial of second order of the form

$$\rho(\theta) = p_1\theta^2 + p_2\theta + p_3 \quad (1)$$

to each contour segment by minimizing the distance between $\rho(\theta)$ and $r(\theta)$, where r is the radius and θ the angle of the point (x, y) in polar coordinates, choosing the center of the plant as the center of the coordinate system. The former is found by computing the centroid of the image foreground of the initial frame, which should contain only the plant. The parameters p_1 , p_2 , and p_3 determine the shape of the polynomial. For each contour segment, we find the point that has the largest fitting error and split the contour at this point. The procedure is terminated when the fitting error is below a predefined threshold γ [30] (see Fig. 2(b)). Parameter values used in the experiments for the different algorithmic parts of the method are provided in Table I.

C. Model-based grouping of contour segments

After having split the initially obtained edge into contour segments s_i , we group the contour segments using a leaf-shape model to obtain leaf detections (see Fig. 2(d)). Since the tobacco leaves at early growth stages have an approximately circular shape, we use a circle as shape model, i.e.,

$$f_i(x, y) = [c_i^2 - (x - a_i)^2 + (y - b_i)^2]^{1/2} \quad , \quad (2)$$

where c_i is the radius of the circle, a_i is the x and b_i the y position of the circle's center. The parameters a_i , b_i , and c_i are found by minimizing the energy

$$E(s_i) = \sum_{(x,y) \in s_i} f_i^2(x, y) \quad (3)$$

for every segment s_i . The circular model can be replaced by other shapes, depending on the plant type that one wishes to analyze.

We further compute for each contour segment s_i the set of pixels A_i that lie within the area of the fitted circle. Then the

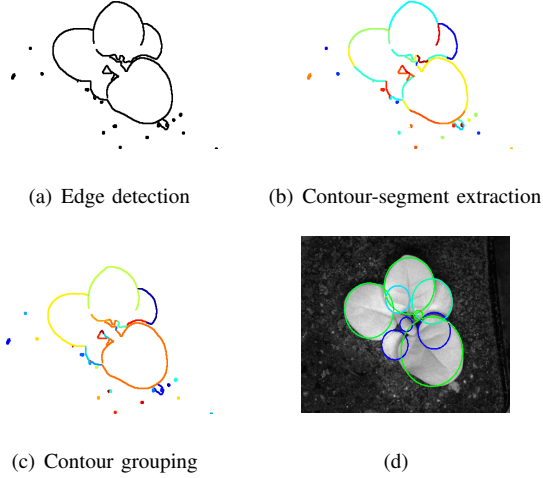


Fig. 2. Consecutive steps for leaf detection. (a) Edge detection, (b) contour-segment extraction, (c) contour-segment grouping, and (d) leaf-shape models fitted to the contour segments with increasing confidences color-coded from dark to light blue.

similarity $w_{ij} := J(A_i, A_j)$ between two contour segments s_i and s_j is defined by the Jaccard coefficient [31]

$$J(A_i, A_j) = \frac{|A_i \cap A_j|}{|A_i \cup A_j|}, \quad (4)$$

which is the ratio between the amount of pixels of the intersection and the union of the two sets.

To merge contour segments that belong to the same leaf within each frame, we define a contour-segment graph (V, e) , where the contour segments define the nodes V of the graph, and e denotes undirectional edges. At the beginning of the procedure, no edges exist between nodes. We compute pairwise similarities w_{ij} between contour segments s_i and s_j if the closest tip points of the contours are less than a threshold δ apart and write them to a list. We sort the similarity values in order of decreasing values. We further define a merging threshold d , which should be chosen in the range between 1 and 0, where 1 corresponds to perfectly matching circles, and 0 to non overlapping circles.

Then the algorithm proceeds as follows:

- (1) We select the first value w_{ij} of the ordered list together with the corresponding contour segments s_i and s_j .
- (2) An edge e_{ij} is created if $w_{ij} > d$. In this case, a new contour segment $s_{i \cup j}$ is created and the respective shape model $f_{i \cup j}$ is found. The shape models of segments s_i and s_j are replaced by the new shape model $f_{i \cup j}$. A flag is set indicating whether the shape-model parameters of a segment have been updated or not. If $w_{ij} \leq d$, nothing needs to be done.
- (3) We select the next value of the ordered list. If one of the corresponding segments has been updated previously and thus flagged, the edge similarity between the segments is recomputed using the current shape models.

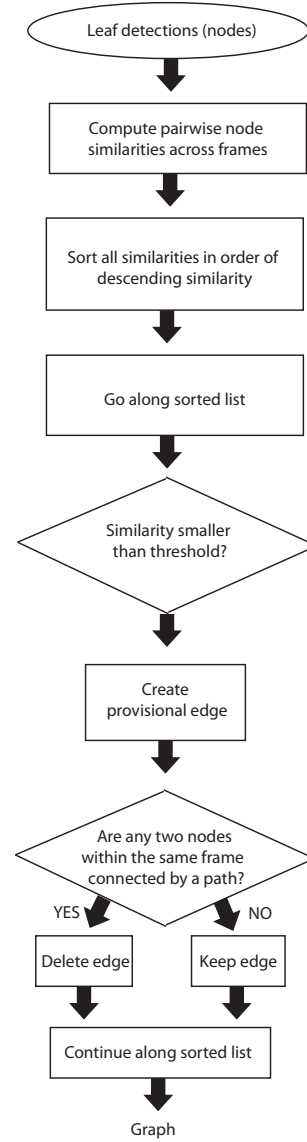


Fig. 3. Flow chart of the graph-based tracking algorithm (explanations in text).

- (4) Step 2-3 are repeated until the first similarity value below threshold is reached.

The final segmentation is then defined by the connected components (subgraphs) of the resulting graph. A result of this merging strategy is depicted in Fig. 2(d).

Working consecutively along the ordered list and updating the shape models along the way allows us to avoid testing for all possible merging combinations, which otherwise could lead to a combinatorial explosion. This strategy gives preference to merges of segments with large similarity. The method is related to Kruskal's algorithm for finding the minimum spanning tree of a graph [29], with the difference that in our case the weights of the graph edges have to be updated during the procedure.

After having grouped the contour segments, we eliminate all contour segments whose contour length is less than a percentage ξ of the fitted contour. Occasionally, contours that

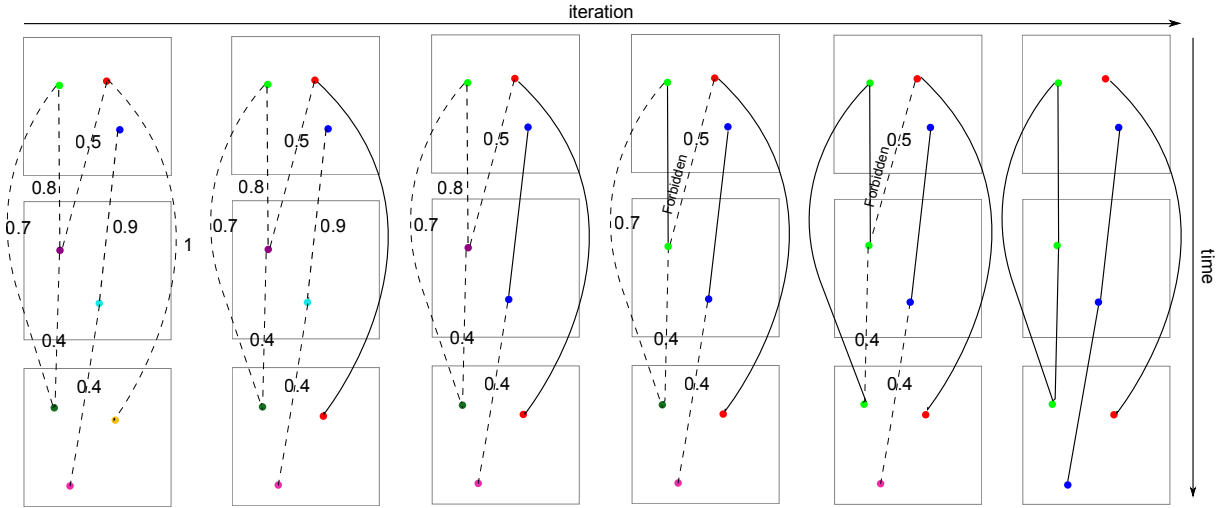


Fig. 4. Graph-building procedure. Leaf detections found for each frame along the sequence define the nodes of the graphs. Nodes that belong to the same connected component are given the same color. We start with the largest similarity value, in the leftmost panel, and draw an edge between the nodes. In the same way, the node pairs with similarities 0.9, 0.8, and 0.7 are connected in the next three iterations. When arriving at the configuration shown in the fifth panel, no edge is drawn between the red node in the upper frame and the light green node in the middle frame because the light green and the red node of the upper frame would be connected by a path. Without this constraint, the algorithm would incorrectly merge different growth tracks. The final result after completing the iterative merging procedure is presented in the last panel. It is assumed that all remaining pairings have a similarity value below threshold. As can be seen, despite gaps in the sequences and noisy similarity values, the algorithm arrives at a solution dividing the sequences of leaf detections into distinct growth tracks, each one representing a subgraph of sequence graph (last panel).

belong to the same leaf are separated by a distance larger than δ . We thus apply a final merging step and force merge all contour segments that have a large overlap (> 0.7). The parameter for forced merging should be larger or equal than d .

D. Leaf tracking

Having identified the main contour segments in each frame according to a leaf-shape model, we want to track the growth of the main leaves of the plant. Each contour segment together with its fitted model shape represents a potential leaf or leaf detection (see Fig. 2(d)). However, due to noise in the images, occlusions, leaf movement, changes during growth, failures in the edge detection or contour extraction, contours may disappear and reappear from one frame to another. In addition, some of the detected contours may not represent a true leaf contour. This means that we still have to identify the main leaves of the plant and track them along the sequence. Given the limitations described above, frame-to-frame tracking is expected to be insufficient to solve the task, instead, we have to consider multiple frames simultaneously in order to bridge gaps in the sequence and identify temporally persistent contours.

We developed a graph-based tracking procedure to address this problem. We build a graph (V^*, e^*) using all frames of the sequence, where the nodes V^* represent the contour segments that resulted from the previous step. Initially, no edges are drawn between nodes, i.e., $e^* = \emptyset$. Similarity values w_{ij} between contour segments that belong to different frames and that are less than σ_1 frames apart are computed and written into a list. The list is sorted in order of descending similarity. Further, a merging threshold d^* is defined.

Then the algorithm proceeds as follows:

- (1) We select the first similarity value w_{ij} of the ordered list and its corresponding contour segments s_i and s_j .
- (2) If $w_{ij} > d^*$, a provisional edge between the nodes is created.
- (3) If any two nodes located in the same frame are connected by a path, the provisional edge is removed. Otherwise, the edge is permanently added to the graph.
- (4) We select the next similarity value of the ordered list.
- (5) Steps 2-3 are repeated until a similarity value below threshold is reached.

Also this method is similar to Kruskal's algorithm for finding the minimum spanning tree of a graph, except for the merging constraint that was incorporated [29] and by which uniqueness of frame-to-frame pairings is assured. Growth tracks are then defined by the connected components (subgraphs) of the graph. A flow chart of the method can be found in Fig. II-B.

We further illustrate the different steps using the example presented in Fig. 4. At the end of the graph-building process, three connected components (denoted by different colors) remain. The length (or number of nodes) of each connected component provides a measure of the persistency of a contour. Assuming that persistent contours correspond to true leaf contours, we can identify the growth tracks of the main leaves of the plant, where we represent the leaf radius c as a function of the discrete time steps t_k .

For the leaf-tracking algorithm to work correctly, it is necessary that leaves coexist over a number of frames in

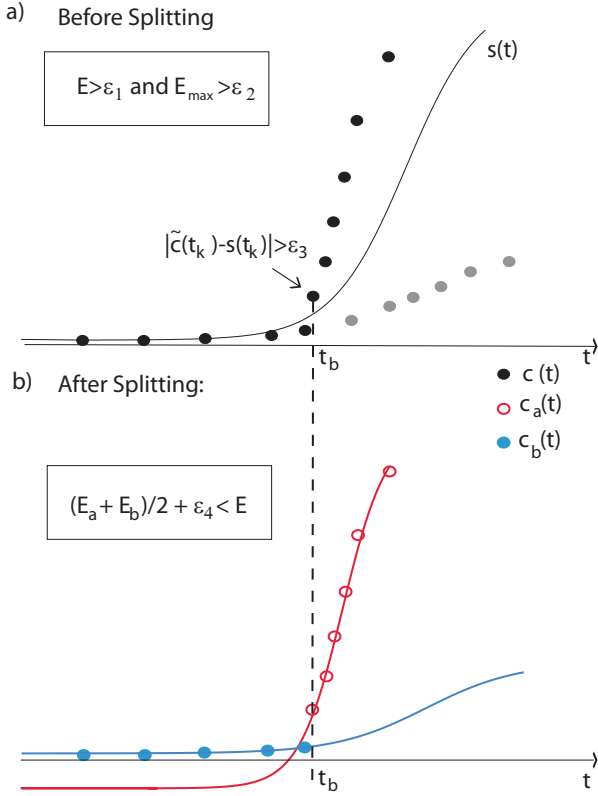


Fig. 5. Schematic illustrating the splitting of growth tracks using fitting errors of growth model. a) If the initially fitted curve $s(t)$ has a large fitting error, the first time point t_b is searched for which the distance of the data to $s(t)$ exceeds a threshold. Black circles indicate leaf detections belonging to the original track. Gray circles indicate the presumed leaf detections that would have been caused by the first leaf if it would not have been occluded. b) The data is splitted at t_b and the split is accepted if the joint error plus a constant ϵ_4 is smaller than the original fitting error. Note that even if the first leaf should reappear due to nastic movements of the occluder, these detections would be assigned to a different, probably spurious growth track.

order to be identified as separate tracks. In cases where a new leaf rapidly occludes another leaf, either by growth or nastic movements, a large similarity may be found across frames for two different leaves when both leaves have reached a similar size, and the two tracks are merged. How these erroneous merges are corrected is explained in the next section.

E. Growth-curve fitting

Growth-curve fitting is required to extract leaf growth parameters from the identified connected components of the graph found in the previous section. Growth tracks $c(t)$ describe how the radius of the fitted circle evolves over time. Once individual growth tracks have been identified, we fit a logistic curve (also called the autocatalytic growth function in [2])

$$s(t) = s_{\max} / [1 + \exp(-g_r(t - \tau))] \quad (5)$$

to each track $c(t_k)$, where s_{\max} , g_r , and τ are parameters characterizing the growth of the leaf and t is time. More exactly, s_{\max} is the maximum radius of the circle modeling

Parameter	Value	Units
Leaf detection		
γ	10	pixels ²
δ	100	pixels
d	0.5	x
ξ	0.4	x
Leaf tracking		
d^*	0.3	x
σ_1	20	frames
Growth-curve fitting		
σ_2	28	frames
ϵ_1	2	pixels
ϵ_2	10	pixels
ϵ_3	5	pixels
ϵ_4	1	pixels

TABLE I
PARAMETER CHOICES FOR THE DIFFERENT ALGORITHMIC STEPS. LENGTH IS MEASURED IN THE IMAGE BY THE NUMBER OF PIXELS.

the leaf, g_r is the growth rate of the constant exponential growth observed for $t \ll \tau$, i.e., the slope of the linear increase of each curve (in logarithmic plots see Fig. 9(b)), and τ is a time offset corresponding to the position of the inflection point of the growth curve. The point in time when a leaf emerges first, cannot be determined from this model without further assumptions. We then compute the mean fitting error as $E = \sum_k |s(t_k) - \tilde{c}(t_k)| / \sum_k 1$ and the maximum fitting error $E_{\max} = \max_k (|s(t_k) - \tilde{c}(t_k)|)$, where $\tilde{c}(t_k)$ is the smoothed growth track, obtained using a sliding window of size σ_2 .

As described in the previous section, two growth tracks belonging to two different leaves may be merged when one leaf occludes the other. This however results in an increasing fitting error because the merged tracks cannot be properly described by a single logistic curve. Hence, we can use the fitting errors to determine incorrect merges of growth tracks and identify the point where the incorrect merge occurred. If $E > \epsilon_1$ and $E_{\max} > \epsilon_2$, then we break the growth track at the point where the data points begin deviating from the fitted curve. This breaking point t_b is identified as the first point t_k along the track for which the distance from the fitted curve $s(t_k)$ is larger than ϵ_3 . After splitting the track into two subtracks $c_a(t)$ with $t \leq t_k$ and $c_b(t)$ with $t > t_k$, we fit a logistic curve to each of them and compute the mean errors E_a and E_b for both tracks. Only if $(E_a + E_b)/2 + \epsilon_4 < E$, the splitting is accepted. We do not revisit the leaf-tracking procedure of the previous section, even though this would have been another possibility. Otherwise, nothing is done and the initial track is kept. A schematic of the procedure is provided in Figure 5.

Other approaches for deciding whether or not splitting the curve could potentially be employed instead. This would perhaps help reducing the number of thresholds required, for example methods using multiple hypothesis testing [32] or Bayesian models [33].

III. RESULTS

We tested the procedure on infrared-image sequences showing the growth of ten tobacco-plant seedlings that were grown under the same experimental conditions. Videos together with

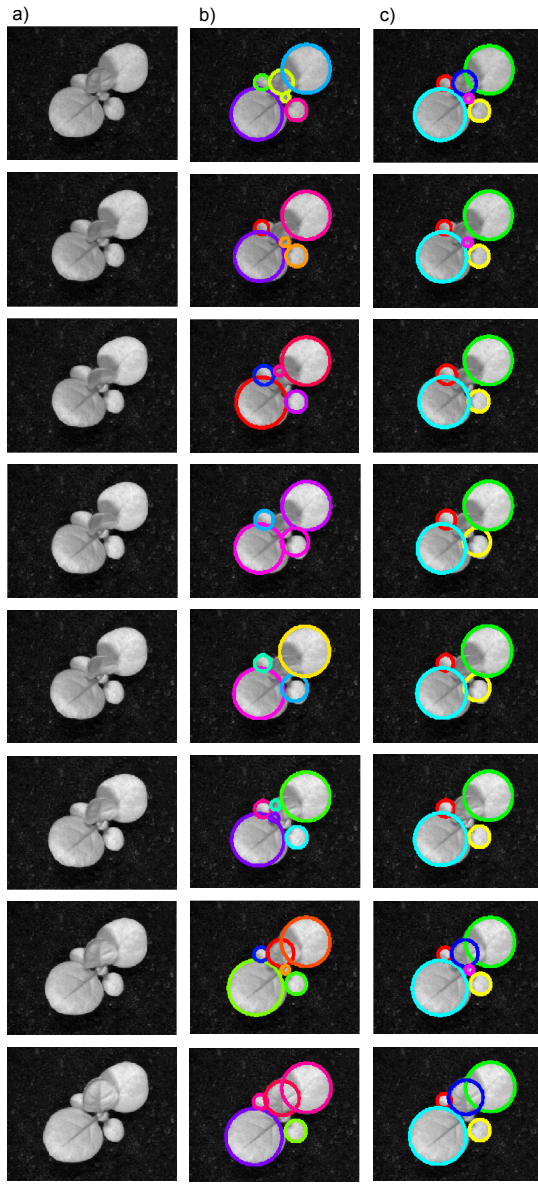


Fig. 6. Tracking example. (a) Original images at 200 to 208 hours of plant 880683. (b-c) Leaf detections before and after tracking is applied, respectively. Leaf detections belonging to the same growth track are assigned the same label, and the fitted leaf-shape models are colored accordingly.

the labeled leaf detections for each frame can be found at www.iri.upc.edu/people/bdellen/PlantGrowth.html. Parameters have been chosen step-by-step such that each component of the algorithm delivered satisfactory and reasonable results. The parameter choices are listed in Table I. Processing times for each frame using a non-optimized Matlab implementation were less than a minute. Before applying the algorithm, we performed a foreground/background segmentation using a fixed threshold to reduce the amount of image edges that have to be processed. This step is not mandatory.

A. Tracking

A major challenge for tracking are those leaves that undergo large nastic movements. In Fig. 6(a), consecutive frames at

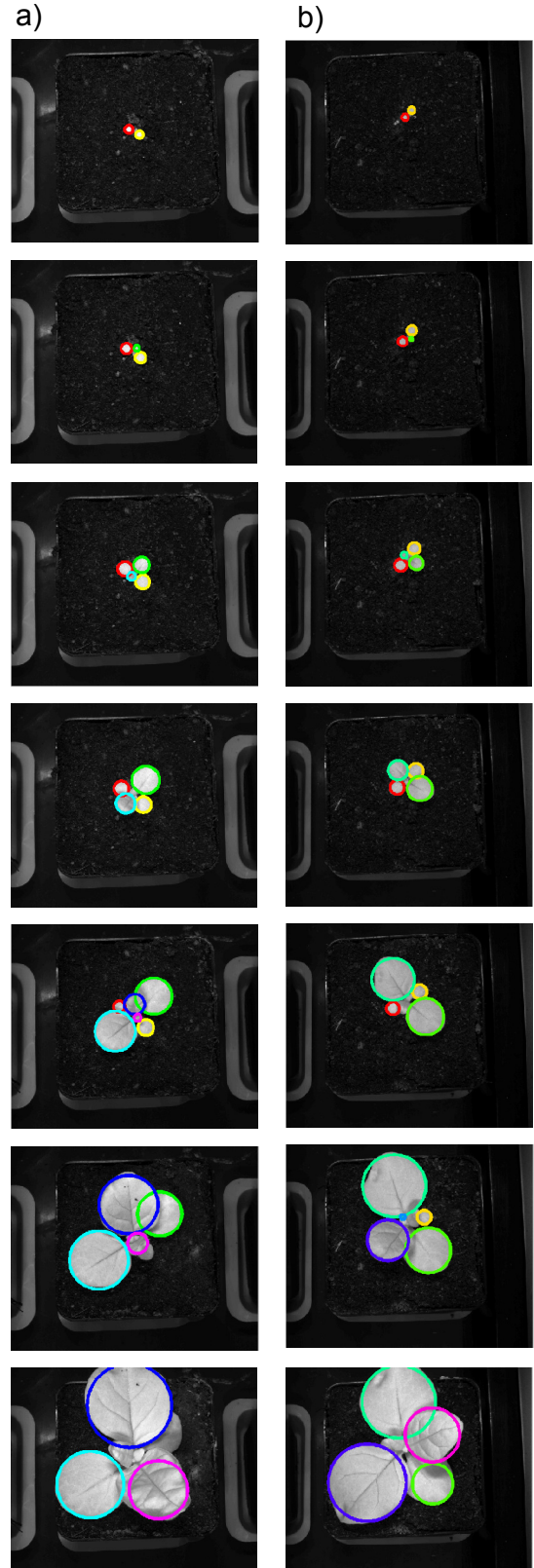


Fig. 7. Tracking results shown for temporally equidistant frames of plants 880683 and 880583. The color-coded fitted circles are overlaid on the original gray scale images. The main leaves of the plants could be tracked successfully.

hours 200 to 208 for plant 880683 (corresponding to a time interval of 8 hours) are shown. As can be seen, due to nastic leaf movements, the central leaf is oriented nearly vertically towards the camera. As a consequence, this leaf is not detected in all frames - see Fig. 6(b), where the leaf detections before applying the graph-based tracking are shown using random colors for the circles overlaid on the images. We further detected false positives occasionally. False positives are more commonly observed at later growth stages when the scene is getting more complex (see Fig. 2(d)).

By means of the tracking procedure, connections are drawn between leaf detections in different frames (see Fig. 6(c)). The labels of the leaf detections and their respective circles are color-coded and overlaid on the original gray-scale images. Tracks that had a size smaller than 20 frames were removed. As we can see, the leaves could be tracked correctly despite the frequent disappearance of leaf detections (particularly of the dark blue one) and false detections that got assigned to spurious, short tracks were filtered out.

In Fig. 7(a-b), we show the results for selected, temporally equidistant frames for plant 880683 and 880583, which represent typical results obtained in the experiments. As we can see, the main leaves of the plant could be tracked successfully. Problems usually arise when a leaf exhibits large motility, and orients its surface vertically towards the camera, making it extremely difficult to detect, particularly when leaves are getting very large. Shadowing and deviation from the assumed circular leaf shape pose additional problems.

In Fig. 8(a), we plot the parameter c of the fitted leaf-shape model of each track as a function of time for plant 880683, plotted as distinctively colored dots, agreeing with the coloring of the leaf detections shown in Fig. 7(a). We further show the logistic function fitted to the individual growth tracks (colored lines). Another typical example (plant 880653) is shown in Fig. 8(b). Commonly, we managed to track the first five to six leaves (including cotyledons) of the plants correctly. Periodic fluctuations in leaf radius around the fitted growth tracks originate from nastic movements, changing the projected size of the leaf in the image. Typical periods were about a day, confirming this assertion.

B. Average growth patterns

The growth patterns of the different plants were highly similar, which allowed us to compute an average growth pattern. For this purpose, we first sorted the growth curves found for each plant in order of appearance (measured by the parameter τ). We further removed all tracks that contained less than 50 data points to remove as many erroneous results as possible. Then we set the parameter τ of the first growth curves (corresponding to the first leaf appearing) to zero. This way, the growth patterns of different plants could be temporally aligned. The aligned growth curves of the different plants are plotted in Fig. 8(c). The first two leaves, i.e. the two cotyledons, which appear at the same time, are shown as yellow and red colors. We treat them as two independent leaves emerging at different points in time, as they may be picked up at different individual times by the algorithm. The third leaf is

Leaf number	s_{\max} [mm]	g_r [1/h]	τ [h]	f_g	count
1	3.02	0.02	0	2.61	10
2	3.6	0.017	11.0	2.26	10
3	9.97	0.02	134.2	2.61	10
4	17.19	0.023	193.5	3.02	10
5	22.7	0.032	240.0	4.65	8
6	64.22	0.022	363.5	2.87	5

TABLE II
PARAMETERS OF THE AVERAGE LOGISTIC CURVES AND RESPECTIVE GROWTH FACTORS. LEAF RADIUS IS GIVEN IN MILLIMETERS.

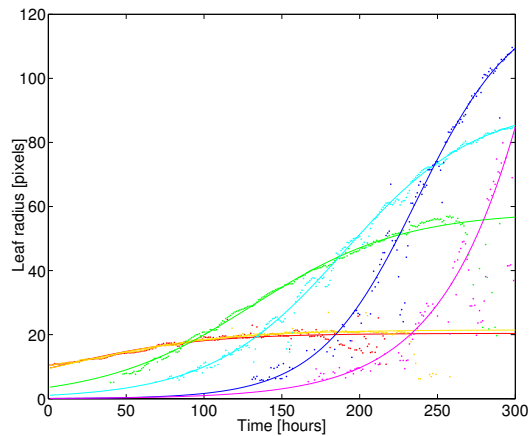
shown in green, the fourth in light blue, the fifth in dark blue, and the sixth in violet. The average growth curve for each leaf is shown in Fig. 9(a), which were obtained by averaging the fitted growth curves, not the model parameters. The respective logarithmic plot is shown in Fig. 9(b). Averaging sequences of growth curves can be problematic if the sequence order is flawed, and more sophisticated methods may have to be employed in the future. The parameters of the logistic curves resulting from averaging the growth curves obtained for different plants are presented in Table II. The growth tracks of the fifth and the sixth leaf were not above threshold in some of the experiments, leading to a count number below 10. We also calculated the growth factor $f_g = \exp(2gt_s)$, measuring the factor of area increase per $t_s = 24$ hours. Average growth curves represent an estimation theoretic mean of the measured plant population. Variance estimates on the model parameter, e.g. the so-called Cramer-Rao-Lower-Bound (see e.g. [34]) then allow defining a metric in the parameter space, e.g. the Mahalanobis distance [35]. They can thus be used to compare groups of plants e.g. under different treatments or featuring different genotypes. They also allow identifying outliers in terms of the model parameters, i.e. detect plants showing unusual growth behavior. They are thus well suited for plant phenotyping, where comparing measured plant performance is a basic requirement.

C. Sensitivity analysis

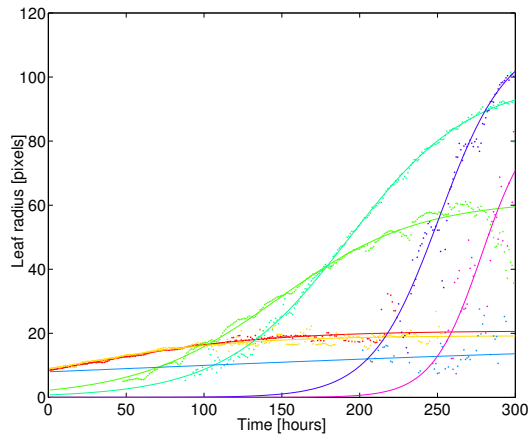
We investigated the sensitivity of the algorithm to the choice of control parameters and the scale of the image. For this purpose, we generated a ground truth for plant 880683 by hand-labeling the center of each leaf for every 20th frame and fitting a logistic curve to the extracted data points (see Fig. 10a). The growth curves estimated by our algorithm are then compared to the ground-truth curves by computing first all pairwise similarities. For a curve i (ground truth) and a curve j (estimated), the similarity is defined as

$$s_{ij} = \exp\left[-\sum_t^n ((c_i(t) - c_j(t))^2/n)/\sigma_3^2\right] \quad , \quad (6)$$

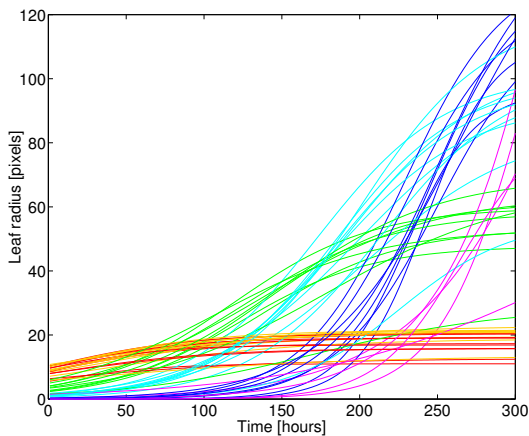
where $\sigma_3 = 4.5$ mm and n is the number of frames of the sequences. The computation of the pairwise similarity matrix yields a confusion matrix S from which we estimated unique correspondences between the two sets of growth curves using a method by Scott and Longuet-Higgins [36]. The similarity values of the “good” pairings are summed and divided by the number of ground-truth curves, providing a performance



(a)

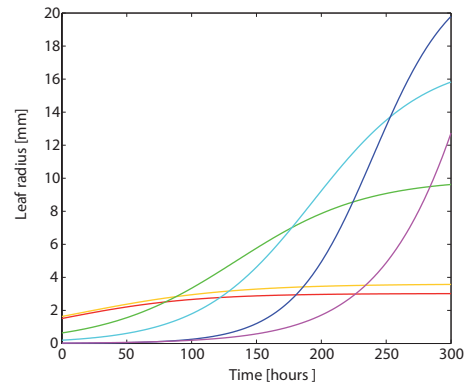


(b)

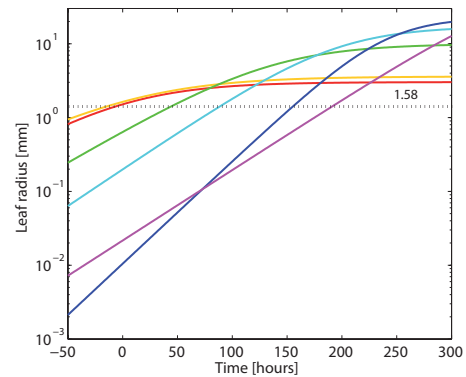


(c)

Fig. 8. Growth curves. (a) The leaf radius c is plotted as a function of time for plant 880683 (colored dots) together with the logistic functions fitted to each growth track (continuous line). The coloring of the growth curves is consistent with the coloring of the leaf detections in previous figures. (b) Growth tracks and curves for plant 880653. (c) Temporally aligned and sorted growth curves for all plants. Each unit of the y axis corresponds to ≈ 0.18 mm.



(a)



(b)

Fig. 9. (a) Averaged growth curves for each leaf, representing the growth signature of the plant, showing leaf radius as a function of time. (b) Log plot of the averaged growth curves. The leaf-radius threshold for computing the phyllochrons (see discussion) is indicated by a dotted line.

measure of the method with scores ranging from 0 to 1 (no match to perfect match). For default parameters (given in Table I) we obtained a score of 0.96. Even after drastically downsizing the images of the sequence by a factor 8, a similar score was obtained, i.e., 0.95. The respective growth curves and confusion matrix are presented in Fig. 10b.

We further were interested in the sensitivity of the algorithm to tracking parameters. Changing the merging threshold d^* only led to a drop in performance for very large thresholds and thus seemed not suitable to tune the performance of the method. The number of frames σ_1 across which links between leaf detections in different frames can be established turned out to have a noticeable impact on the results. For $\sigma_1 = 3$ frames, i.e., only direct neighbors are considered, the performance dropped to 0.84. We further investigated the robustness to noise in dependence of σ_1 frames. In the tracking procedure, we reduced the pairwise similarities by adding equally distributed random values between 0 and η . For each noise level and parameter σ_1 , we used five different instantiations of the noise to compute average performance values. As can be seen in Table III, the performance of the method for $\sigma_1 = 3$ frames dropped rapidly with increasing noise level. For $\sigma_1 = 20$ frames, the method was hardly affected by the noise.

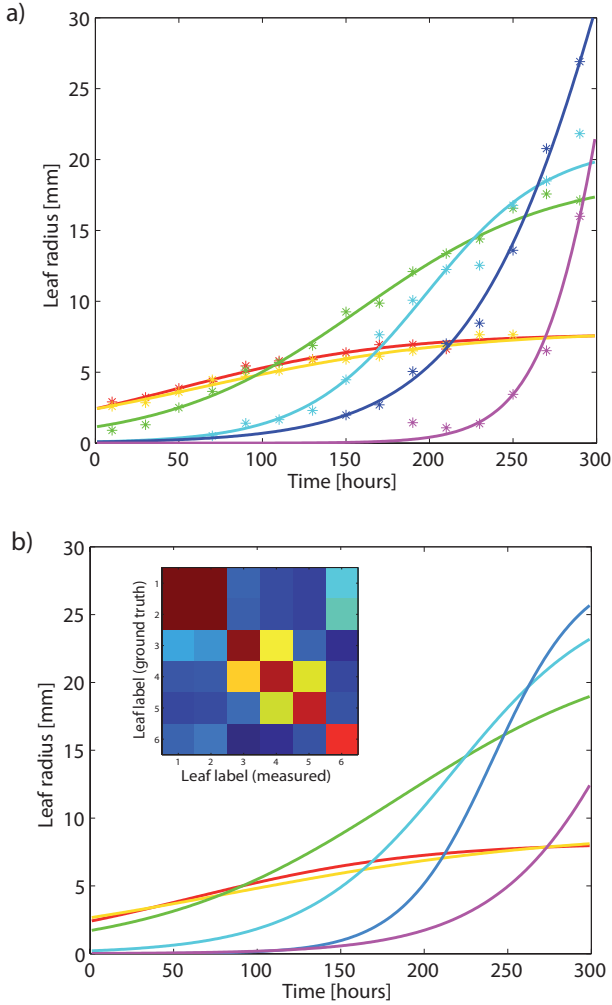


Fig. 10. a) Ground-truth growth curves for plant 880683. b) Growth curves estimated from downscaled images with a factor 8. The respective confusion matrix with ground truth (inset) shows the similarities computed between the measured and the ground-truth growth tracks of the plant (values are color coded from dark blue to red, where blue represents low values, red large ones, and yellow intermediate ones).

σ_1	$\eta = 0$	$\eta = 0.5$	$\eta = 1$
20	0.96	0.89 ± 0.05	0.87 ± 0.04
10	0.88	0.83 ± 0.11	0.76 ± 0.09
3	0.84	0.72 ± 0.04	0

TABLE III

TRACKING PERFORMANCE (FROM 0 TO 1) FOR PLANT 880683 IN DEPENDENCE OF TRACKING PARAMETER σ_1 FOR DIFFERENT NOISE LEVELS η . A LARGE σ_1 INCREASES ROBUSTNESS OF THE ALGORITHM.

By being able to create links between distant frames, errors in the graph can be better compensated, and “bad” detections can be averaged out. Intermediate results were obtained for $\sigma_1 = 10$ frames.

IV. DISCUSSION

In this work, we presented a novel graph-based tracking algorithm based on Kruskal’s method which permits finding

and following the first leaves of a plant during growth from a sequence of noisy leaf detections. Initial leaf detections were obtained by first extracting contour segments from the infrared images, then grouping them using a leaf-shape model. From the leaf detections, a graph was built where edges were drawn between edges dependent on the pairwise similarities of fitted leaf-shape models across frames. By incorporating a unique-matching constraint into a method for finding the minimum spanning tree in a graph [29], the main leaf tracks could then be identified by finding the connected components of the resulting graph. Since graph edges were allowed to span across many frames, it was possible to bridge gaps in the sequence of leaf detections.

We tested the method on a set of tobacco-plant growth sequences, showing the first two weeks of growth of tobacco seedlings. The algorithm succeeded in tracking the main leaves of the plants despite considerable nastic leaf movements and growth, which changed the appearance of the leaves in the image and made them hard to detect at times, particularly when leaves were moving out of the image plane, pointing in the direction of the camera, or occluding others.

As typical for dicotyledons, cotyledons would become visible to the algorithm at approximately the same time and grow with very similar dynamics in opposing directions (see Fig. 9(a), yellow and red curves). After two days (see Fig. 8(a,b), measurements for the green line) the first true leaf would appear. From Table II we see, that this leaf grows at the same rate as the cotyledons, but stays considerably longer in the exponential growth phase. It reaches the inflection point 5.5 days (134.2 hours) later than the cotyledons (green track in Fig. 9(a)). The second true leaf (light blue curve in Fig. 9(a), leaf number 4 in Table II) would be picked up by the algorithm after 3 to 4 days, grow a little faster than the previous leaf, and stay in the exponential growth phase about 1 day longer, as it appears 1-2 days after the previous leaf, but reaches its inflection point ≈ 60 hours later. The growth rate g_r of leaf 5 (true leaf 3, dark blue tracks in Fig. 9) is again larger than that of the leaves before, but the exponential growth period did not increase. For leaf 6 (true leaf 4, violet tracks in Fig. 9), we observe high variance in our data (cmp. Fig. 8(c)), reducing descriptive power of our findings for this leaf. However, we clearly see that also this leaf becomes larger than its predecessors and grows at a comparable rate and duration. The observed growth pattern seems to be very robust. Similar patterns have been described before for leaf elongation of e.g. *Capsicum frutescens* [37], wheat [8], *Arabidopsis thaliana* [38], or *Ficus formosana* [39]. From Figure 9(b) we can read the phyllochrons as durations between the time points, when leaves reach a certain size. We select size 1.58 mm, as this yields the minimum duration between cotyledon emergence, which ideally should be zero, and calculate phyllochrons from the values given in Table II using the inverse of the autocatalytic growth model. Phyllochrons are then between the cotyledons -8 h, and 54 h, 43 h, 65 h, 37 h for the following leaves. We observe that the first 2 leaves after the cotyledons emerge relatively quickly, the next leaf emerges with a short delay and the following leaf then emerges quicker again. The same characteristic can be read e.g. from Figure 5 in [28]. The

proposed algorithm makes this kind of measurements available to automated phenotyping procedures, as e.g. proposed in [40], [5], [41], [42]. Preliminary results indicate that growth tracks can be found by the method also when downsizing the image by a factor 8, suggesting that the method could be used also together with low-resolution (low-cost) cameras, for example in applications using the Kinect RGB-D camera [43]. However, the choice of the set-up may also depend on the type of the plant that is being analyzed, and the amount of details that one wants to extract.

The limitations of our approach lie in the reliance on a simple circular model for leaf fitting and on a set of parameters that need to be adjusted depending on the imaging data. For example, *Arabidopsis*, which is another popular model plant, has leaf shapes that deviate from the circular shape assumed in our method. In principle, other leaf-shape models could be accommodated by our approach, but model fitting may be more elaborate particularly when the model contains many parameters. The structures and detailed shapes of leaves could be approximated by polygons whose vertices are critical curvature points of leaf contours as it was done in [44]. Also spline-based shape-spaces as introduced in [45] may be applied in order to represent more elaborate shapes with a minimum number of free parameters. Perhaps components of the method could be replaced in the future by parameter-free methods or parameters could be learned, for example by creating ground-truth growth curves for a few examples (requiring hand-labeling of leaves), and then maximizing the performance measure. However, despite the discussed limitations of the approach, it provides a solution to a difficult problem, and demonstrates that the monitoring of leaf growth can be feasible under certain conditions.

Graph-based methods have been widely used in various applications, ranging from object tracking to video segmentation. While former methods mostly use graphs to find matches in subsequent frames [46], the video-segmentation algorithm by Grundmann et al. (2010) builds a region graph and computes a tree of spatiotemporal segmentations [47]. However, since the task there was a different one, no unique-matching constraint was incorporated.

Further investigations will be necessary to elucidate the usefulness of variations in this growth pattern as phenotypic trait and its relation to changing environmental conditions and genotypes. We hope and believe that the achieved automated measurement of this characteristic growth signature cannot only be used to monitor, but also to control plant growth in plant production.

V. ACKNOWLEDGEMENTS

The research leading to these results has received funding from the European Commission Seventh Framework Programme FP7/2007-2013 Challenge 2 Cognitive Systems, Interaction, Robotics under grant agreement No 247947 GARNICS. B. Dellen acknowledges support from the Spanish Ministry for Science and Innovation through a Ramon y Cajal program.

REFERENCES

- [1] D. Houle, D. R. Govindaraju, and S. Omholt, "Phenomics: the next challenge," *Nature Review Genetics*, vol. 11, no. 12, pp. 855–866, Dec. 2010.
- [2] F. J. Richards, "A flexible growth function for empirical use," *J. Exp. Bot.*, vol. 10, no. 2, pp. 290–301, 1959.
- [3] D. R. Causton, "Some mathematical properties of growth curves and applications to plant growth analysis," Ph.D. dissertation, 1967.
- [4] R. Hunt, "Plant growth analysis: The rationale behind the use of the fitted mathematical function," *Annals of Botany*, vol. 43, pp. 245 – 249, 1979.
- [5] A. Walter, H. Scharf, F. Gilmer, R. Zierer, K. A. Nagel, M. Ernst, A. Wiese, O. Virnich, M. M. Christ, B. Uhlig, S. Jünger, and U. Schurr, "Dynamics of seedling growth acclimation towards altered light conditions can be quantified via growSCREEN: a setup and procedure designed for rapid optical phenotyping of different plant species," *New Phytologist*, vol. 174, no. 2, pp. 447–455, 2007. [Online]. Available: <http://dx.doi.org/10.1111/j.1469-8137.2007.02002.x>
- [6] U. Schurr, A. Walter, and U. Rascher, "Functional dynamics of plant growth and photosynthesis—from steady-state to dynamics—from homogeneity to heterogeneity," *Plant Cell Environ.*, vol. 29, no. 3, Mar. 2006. [Online]. Available: <http://www.ncbi.nlm.nih.gov/pubmed/17080590>
- [7] A. Walter and U. Schurr, "The modular character of growth in nicotiana tabacum plants under steady-state nutrition," *Journal of Experimental Botany*, vol. 50, no. 336, p. 1169, 1999.
- [8] G. Beemster, J. Masle, R. Williamson, and G. Farquhar, "Effects of soil resistance to root penetration on leaf expansion in wheat (*triticum aestivum* L.): Kinematic analysis of leaf elongation," *Journal of Experimental Botany*, vol. 47, pp. 1663–1678, 1996.
- [9] P. Donnelly, D. Bonetta, H. Tsukaya, R. Dengler, and N. Dengler, "Cell cycling and cell enlargement in developing leaves of *arabidopsis*," *Developmental Biology*, vol. 215, pp. 407–419, 1999.
- [10] W. Sadok, P. Naudin, B. Boussuge, B. Muller, C. Welcker, and F. Tardieu, "Leaf growth rate per unit thermal time follows qtl-dependent daily patterns in hundreds of maize lines under naturally fluctuating conditions," *Plant Cell Environ.*, vol. 30, no. 2, pp. 135–146, Feb 2007.
- [11] R. Poire, A. Wiese-Klinkenberg, B. Parent, M. Mielewicz, U. Schurr, F. Tardieu, and A. Walter, "Diel time-courses of leaf growth in monocot and dicot species: endogenous rhythms and temperature effects," *Journal of Experimental Botany*, vol. 61, no. 6, pp. 1751–1759, 2010.
- [12] D. Schmundt, M. Stitt, B. Jähne, and U. Schurr, "Quantitative analysis of the local rates of growth of dicot leaves at a high temporal and spatial resolution, using image sequence analysis," *Plant J.*, vol. 16, pp. 505–514, 1998.
- [13] A. Wiese, M. Christ, O. Virnich, U. Schurr, and A. Walter, "Spatio-temporal leaf growth patterns of *arabidopsis thaliana* and evidence for sugar control of the diel leaf growth cycle," *New Phytol.*, vol. 174, p. 752761, 2007.
- [14] R. Furbank and M. Tester, "Phenomics – technologies to relieve the phenotyping bottleneck," *Trends in Plant Science*, vol. 16, no. 12, pp. 635–644, 2011.
- [15] E. Spalding and N. Miller, "Image analysis is driving a renaissance in growth measurement," *Current Opinion in Plant Biology*, vol. 16, no. 1, pp. 100–104, 2013.
- [16] C.-H. Teng, Y.-T. Kuo, , and Y.-S. Chen, "Leaf segmentation, classification, and three-dimensional recovery from a few images with close viewpoints," *Optical Engineering*, vol. 50, no. 3, pp. 1–12, 2011.
- [17] L. Quan, P. Tan, G. Zeng, L. Yuan, J. Wang, and S. Kang, "Image-based plant modelling," *ACM Siggraph*, pp. 599–604, 2006.
- [18] Y. Song, R. Wilson, R. Edmondson, and N. Parsons, "Surface modelling of plants from stereo images," *6th IEEE Intl. Conf. on 3D Digital Imaging and Modelling*, pp. 312 – 319, 2007.
- [19] B. Loch, J. Belward, and J.S.Hanan, "Application of surface fitting techniques for the representation of leaf surfaces," *MODSIM 2005 International Congress on Modelling and Simulation*, pp. 1272–1278, 2005.
- [20] G. Alenyà, B. Dellen, and C. Torras, "3d modelling of leaves from color and tof data for robotized plant measuring," *Proc. IEEE Intl. Conf. on Robotics and Automation*, pp. 3408–3414, 2011.
- [21] T. B. Moeslund, M. Aagaard, and D. Lerche, "3d pose estimation of cactus leaves using an active shape model," in *WACV/MOTIONS'05*, vol. 1, 2005, pp. 468–473.
- [22] L. Silva, M. Koga, C. Cugnasca, and A. Costa, "Comparative assessment of feature selection and classification techniques for visual inspection of

- pot plant seedlings,” *Computers and Electronics in Agriculture*, vol. 97, pp. 47–55, 2013.
- [23] J. Wang, J. He, Y. Han, C. Ouyang, and D. Li, “An adaptive thresholding algorithm of field leaf image,” *Computers and Electronics in Agriculture*, vol. 96, pp. 23–39, 2013.
- [24] G. Alenya, B. Dellen, S. Foix, and C. Torras, “Robotized plant probing: Leaf segmentation utilizing time-of-flight data,” *Robotics Automation Magazine, IEEE*, vol. 20, no. 3, pp. 50–59, Sept 2013.
- [25] B. Biskup, H. Scharr, U. Schurr, and U. Rascher, “A stereo imaging system for measuring structural parameters of plant canopies,” *Plant, Cell and Environment*, vol. 30, pp. 1299–1308, 2007.
- [26] G. Polder, G. van der Heijden, H. Jalink, and J. Snel, “Correcting and matching time sequence images of plant leaves using penalized likelihood warping and robust point matching,” *Computers and Electronics in Agriculture*, vol. 55, no. 1, pp. 1–15, 2007.
- [27] M. Minervini, M. M. Abdelsamea, and S. A. Tsafaris, “Image-based plant phenotyping with incremental learning and active contours,” *Ecological Informatics (in press)*, 2013.
- [28] C. H. Tsai, A. Miller, M. Spalding, and S. Rodermel, “Source strength regulates an early phase transition of tobacco shoot morphogenesis,” *Plant Physiol*, vol. 115, no. 3, pp. 907–914, 1997.
- [29] J. Kruskal, “On the shortest spanning subtree of a graph and the traveling salesman problem,” *Proceedings of the American Mathematical Society*, vol. 7, no. 1, pp. 48–50, 1956.
- [30] R. Duda and P. Hart, *Pattern classification and scene analysis*. Wiley, New York, 1972.
- [31] M. Levandowsky and D. Winter, “Distance between sets,” *Nature*, no. 5323, p. 3435, 1971.
- [32] D. K. Prasad, M. K. H. Leung, and S.-Y. Cho, “Edge curvature and convexity based ellipse detection method,” *Pattern Recogn.*, vol. 45, no. 9, pp. 3204–3221, Sept. 2012.
- [33] K. Katanani, “Uncertainty modeling and model selection for geometric inference. pattern analysis and machine intelligence,” *Pattern Analysis and Machine Intelligence, IEEE Transactions on*, vol. 26, no. 10, pp. 1307–1319, 2004.
- [34] S. M. Kay, *Fundamentals of Statistical Signal Processing: Estimation Theory*. Upper Saddle River, NJ, USA: Prentice-Hall, Inc., 1993.
- [35] P. Mahalanobis, “On the generalised distance in statistics,” in *Proceedings of the National Institute of Science of India*, vol. 2, no. 1, 1936, p. 4955.
- [36] G. Scott and H. Longuet-Higgins, “An algorithm for associating the features of two patterns,” *Proc. Royal Society London B*, vol. 244, pp. 21–26, 1991.
- [37] B. T. Steer, “The dynamics of leaf growth and photosynthetic capacity in capsicum frutescens l.” *Annals of Botany*, vol. 35, no. 5, pp. 1003–1015, 1971.
- [38] P. M. Donnelly, D. Bonetta, H. Tsukaya, R. E. Dengler, and N. G. Dengler, “Cell cycling and cell enlargement in developing leaves of arabidopsis,” *Developmental biology*, vol. 215, no. 2, Nov. 1999. [Online]. Available: <http://dx.doi.org/10.1006/dbio.1999.9443>
- [39] C.-C. Chen, H. Chen, and Y.-r. Chen, “A new method to measure leaf age: Leaf measuring-interval index,” *American Journal of Botany*, vol. 96, no. 7, pp. 1313–1318, July 2009. [Online]. Available: <http://dx.doi.org/10.3732/ajb.0800303>
- [40] C. Granier, L. Aguirrezabal, K. Chenu, S. J. Cookson, M. Dauzat, P. Hamard, J.-J. Thioux, G. Rolland, S. Bouchier-Combaud, A. Lebaudy, B. Muller, T. Simonneau, and F. Tardieu, “Phenopsis, an automated platform for reproducible phenotyping of plant responses to soil water deficit in arabidopsis thaliana permitted the identification of an accession with low sensitivity to soil water deficit,” *New Phytologist*, vol. 169, no. 3, pp. 623–635, Jan. 2006. [Online]. Available: <http://dx.doi.org/10.1111/j.1469-8137.2005.01609.x>
- [41] M. Jansen, F. Gilmer, B. Biskup, K. Nagel, U. Rascher, A. Fischbach, S. Briem, G. Dreissen, S. Tittmann, S. Braun, I. D. Jaeger, M. Metzloff, U. Schurr, H. Scharr, and A. Walter, “Simultaneous phenotyping of leaf growth and chlorophyll fluorescence via GROWSCREEN FLUORO allows detection of stress tolerance in Arabidopsis thaliana and other rosette plants,” *Functional Plant Biology, Special Issue: Plant Phenomics*, vol. 36, no. 10/11, pp. 902–914, 2009.
- [42] T. Dornbusch, S. Lorrain, D. Kuznetsov, A. Fortier, R. Liechti, I. Xenarios, and C. Fankhauser, “Measuring the diurnal pattern of leaf hyponasty and growth in arabidopsis a novel phenotyping approach using laser scanning,” *Functional Plant Biology*, vol. 39, no. 11, pp. 860–869, 2012.
- [43] J. Han, L. Shao, D. Xu, and J. Shotton, “Enhanced computer vision with microsoft kinect sensor: A review,” *Cybernetics, IEEE Transactions on*, vol. 43, no. 5, pp. 1318–1334, Oct 2013.
- [44] C. Im, H. Nishida, and T. Kunii, “Recognizing plant species by leaf shapes—a case study of the acer family,” in *Pattern Recognition, 1998. Proceedings. Fourteenth International Conference on*, vol. 2, Aug 1998, pp. 1171–1173 vol.2.
- [45] A. Blake and M. Isard, *Active Contours: The Application of Techniques from Graphics, Vision, Control Theory and Statistics to Visual Tracking of Shapes in Motion*, 1st ed. Secaucus, NJ, USA: Springer-Verlag New York, Inc., 1998.
- [46] H.-T. Chen, H.-H. Lin, and T.-L. Liu, “Multi-object tracking using dynamical graph matching,” in *In Proc. of IEEE Computer Society Conference on Computer Vision and Pattern Recognition*, 2001, pp. 210–217.
- [47] M. Grundmann, V. Kwatra, M. Han, and I. Essa, “Efficient hierarchical graph-based video segmentation,” in *Computer Vision and Pattern Recognition (CVPR 2010)*, 2010.